9 June 2000

ELSEVIER

Chemical Physics Letters 323 (2000) 105–110

CHEMICAL PHYSICS LETTERS

www.elsevier.nl/locate/cplett

193 nm photodissociation of carbonyl cyanide $CO(CN)_2$ probed by the $CN(v, J)$ fragment

Qiang Li, Robert T. Carter, J. Robert Huber *

Physikalisch-Chemisches Institut der Universität Zürich, Winterthurerstrasse 190, CH-8507 Zürich, Switzerland

Received 23 March 2000

Abstract

The photodissociation of $CO(CN)_2$ at 193 nm has been studied by probing the nascent CN fragments. Two energetically different CN species were identified, a rotationally and vibrationally hot one characterized by $T_r \sim 2300$ K and $T_v \sim 3600$ K, and a cold one exclusively in $v = 0$ with $T_r \sim 410$ K. The hot CN together with OCCN stems from the α-cleavage while the cold CN, which accounts for about 18% of all CN fragments, is from the spontaneous secondary decay OCCN → CN + CO thus confirming the three-body decay to be a sequential process.

1. Introduction

As the simplest ketone, the photochemistry of acetone has been studied extensively [1–4]. Acetone provides a simple case for studying multiple dissociation events of two equivalent bonds including the issue of whether dissociation occurs in a concerted three-body process or in a stepwise manner [5]. Replacing the methyl groups by cyano groups, carbonyl cyanide $CO(CN)_2$ is obtained. This acetone-related molecule has recently been investigated by photofragment translational energy spectroscopy (PTS) [6] resulting in the detection of the CO, CN, OCCN, and NCCN species and their kinetic energy distributions. Based on these findings two decay channels could be identified with the dominant one $(94 \pm 2\%)$ being the α-cleavage or 'radical channel'

$$CO(CN)_2 + h\nu \rightarrow OCCN + CN. \quad (1a)$$

The second decay channel generates, with a yield of $6 \pm 2\%$, molecular species,

$$CO(CN)_2 + h\nu \rightarrow CO + NCCN \quad (2)$$

and is thus reminiscent of the 'molecular decay' in formaldehyde, H_2CO [7]. In addition a fraction of $18 \pm 6\%$ of the nascent OCCN fragments emerging from (1a) have sufficient internal energy to overcome the barrier to the secondary decay

$$OCCN \rightarrow CO + CN \quad (1b)$$

revealing the three-body decay to be a sequential reaction. The lack of any anisotropy ($\beta = 0$) in the recoil distributions as found for the products CN, OCCN, and NCCN in (1a) and (2) suggest that both the radical and the molecular decay are slow and probably indirect [6].

Ab initio calculations [8] were carried out in order to elucidate the energetics and the transition states involved in the reaction path (1a) and particularly in the molecular decay (2). It was assumed that the initially excited state is not dissociative but rather the

* Corresponding author. Fax: +41-1-635-6838; e-mail: jrhuber@pci.unizh.ch

0009-2614/00/$ - see front matter
PII: S0009-2614(00)00505-4

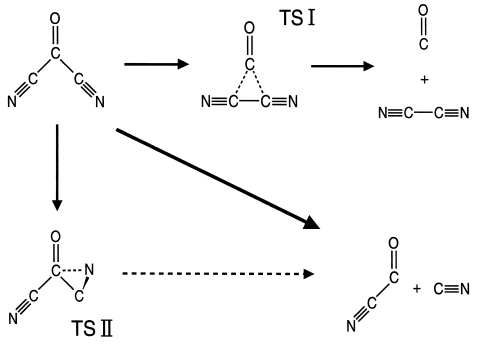

Fig. 1. The three decay paths (radical or α-cleavage decay, molecular elimination and isomerization) of $CO(CN)_2$ after absorption of an UV photon and conversion to the ground state. The transition states TS I and TS II are 460 and 215 kJ/mol above the ground state of the parent molecule, respectively. The α-cleavage with $D_0 \sim 410$ kJ/mol involves no exit channel barrier [8].

electronic ground state of $CO(CN)_2$. Fig. 1 shows the radical decay with the bond dissociation energy D_0(NC–COCN) predicted to be 410 kJ/mol and having no barrier in the exit channel. Two transition states were identified, the planar TS I (460 kJ/mol) along the molecular elimination path and the nonplanar TS II (216 kJ/mol) along the isomerization path. For the latter which is energetically favorable, evidence has been found in matrix photodissociation [8,9].

In the present study the photodissociation of $CO(CN)_2$ has been reinvestigated following excitation at 193 nm. CN ($X^2\Sigma^+$) photofragments were probed via laser induced fluorescence (LIF) to determine the rotational and vibrational state distributions as well as the rotational alignment. In combination with our previous PTS results [6] mechanistic features of the α-cleavage including the secondary photodissociation process were assessed.

2. Experiment

The experimental setup used for this work has been described in detail elsewhere [10,11]. Carbonyl cyanide was synthesised and purified according to a published procedure [12]. Premixed gas samples of 2% $CO(CN)_2$ in 600 mbar He were expanded through a 0.5 mm aperture attached to a piezoelectric pulsed valve into a vacuum chamber of 3×10^{-7} mbar. The expansion conditions were chosen such as to avoid the formation of $CO(CN)_2$ dimers and clusters. Photolysis at 193 nm was performed with an ArF excimer laser (Lambda Physik EMG 101 MSC). The softly focussed laser beam crossed the molecular beam at right angles 60 mm downstream from the nozzle. A counterpropagating probe laser beam recorded the nascent CN photofragments on the $B^2\Sigma^+ \leftarrow X^2\Sigma^+$ system (vibrational bands with $\Delta v = 0$) by LIF. The probe laser, having a linewidth of 0.4 cm^{-1}, was a Lambda Physik dye laser (FL2002) pumped by an XeCl excimer laser (Lambda Physik LPX200) operated with QUI dye between 375 and 390 nm.

Fluorescence from the CN fragments was measured at right angles to the plane of the molecular and laser beams by a Hamamatsu R928 photomultiplier tube (PMT) equipped with an appropriate cutoff filter. Stray light was minimized by delaying the probe laser pulse by 150 ns from the dissociation laser pulse. The photomultiplier signal was fed to a digital boxcar integrator (Stanford Research SR 250), and photodiodes monitored the photolysis and probe laser intensities to correct for shot to shot fluctuations. For the dissociation laser the signal was found to be linear in the range 5–25 mJ/cm^2 and a value of 10 mJ/cm^2 was used, while for the probe laser a power density of 0.2 mJ/cm^2 was chosen to avoid saturation effects. Linearly polarized light at an arbitrary angle for dissociation was generated by passing the excimer laser beam through a stack of 10 quartz plates at Brewster's angle, resulting in a polarization degree of 92%. For the probe beam (polarization 97%) a $\lambda/2$ plate was used. The polarization geometry was chosen as described elsewhere [10,11]. For the linewidth measurements the probe laser was operated with an intracavity etalon providing $\Delta v = 0.11 \pm 0.01$ cm^{-1}.

3. Results and analysis

3.1. CN photofragment distributions

Fig. 2 shows the $B^2\Sigma^+ \leftarrow X^2\Sigma^+$ ($\Delta v = 0$) fluorescence excitation spectrum of the CN ($X^2\Sigma^+$)

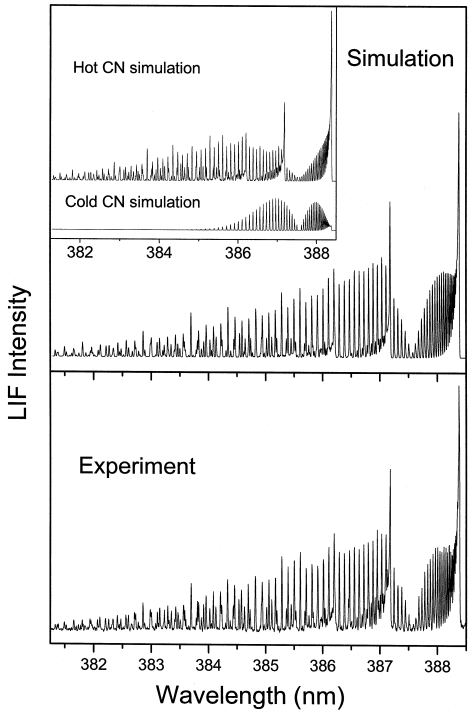

Fig. 2. Bottom: experimental laser-induced fluorescence spectrum of nascent CN $B^2\Sigma^+ - X^2\Sigma^+$ ($\Delta v = 0$) following 193 nm photodissociation of $CO(CN)_2$. Top: simulated LIF spectrum of CN consisting of a superposition of cold and hot CN species in a ratio of 18:82. The inset shows the simulated LIF spectra of the rotationally hot and cold CN contributions.

photofragment resulting from the 193 nm dissociation of carbonyl cyanide. The CN line positions were assigned by reference to recently published assignments and spectral constants [13]. The spectrum shows evidence of significant vibrational excitation; rovibrational transitions from $v = 0$, 1, 2, and 3 are discernible but none from $v = 4$. Using the appropriate Hönl–London and Franck–Condon factors [14], the relative rotational and vibrational populations were extracted from the intensity data. This is illustrated for CN ($v'' = 0$–2) in Fig. 3 where the rotational state distributions are given as Boltzmann plots. For the analysis only non-overlapping rotational transitions were considered. Inspection of the results for CN in $v = 1$ and $v = 2$ shows the plots to be linear corresponding to a rotational temperature T_r of 2400 K and 2300 K, respectively. In the case of $v = 0$, however, we find the data to be well described by *two rotational distributions*, one with $T_r = 410$ K and one with $T_r = 2300$ K. We confirmed that the rotationally cold distribution for CN in $v = 0$ is not due to rotational relaxation by taking measurements with varying delays (35–200 ns) between dissociation and probe laser. The relative intensities of the two components were found to be independent of the delay.

The rotational populations with the appropriate Franck–Condon factors [14] provided the relative vibrational populations using the LIFBASE simulation program [15]. Based on the rotationally hot CN fragments, the vibrational population ratios were thus found to be $P(v = 0):P(v = 1):P(v = 2):P(v = 3) = 0.58:0.26:0.13:0.04$, which conforms to a Boltzmann distribution with a vibrational temperature $T_v = 3600 \pm 200$ K as demonstrated in Fig. 4. The simulations of the CN spectra Fig. 2 (top) revealed that the rotationally cold distribution, which occurs exclusively in $v = 0$, accounts for $18 \pm 2\%$ of all CN

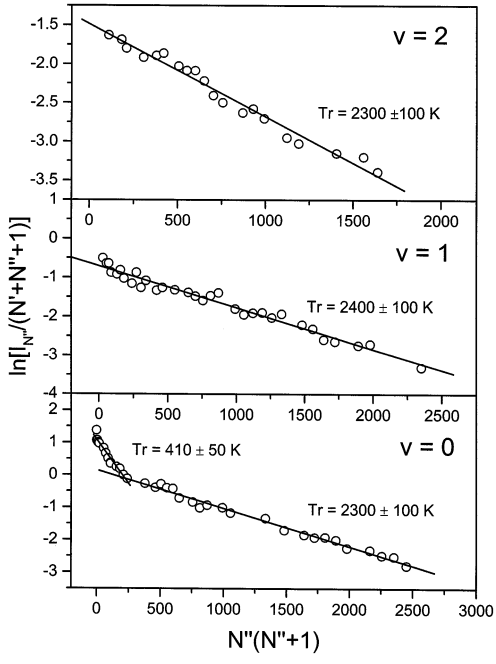

Fig. 3. Boltzmann plots of the rotational state distribution of nascent CN ($X^2\Sigma^+$, $v = 0$–2) from photolysis of $CO(CN)_2$ at 193 nm. The solid lines represent the best fits.

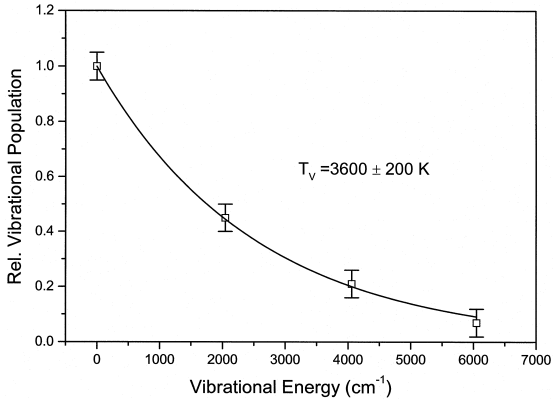

Fig. 4. Vibrational state distribution for rotationally hot CN fragments from the 193 nm photodissociation of $CO(CN)_2$. The solid line represents the best fit of a Boltzmann distribution with a temperature of 3600 K.

fragments; the remaining 82% of the CN fragments are hot.

3.2. Product energy distribution

The available energy, E_{avl}, partitioned among the degrees of freedom of the primary photoproducts CN + OCCN following reaction (1a) is given by

$$E_{avl}(\mathrm{CN}+\mathrm{OCCN}) = h\nu + E_{int}(\mathrm{CO(CN)_2}) - D_0(\mathrm{NC{-}COCN}). \quad (3)$$

The energy of the photon $h\nu$(193 nm) is 619 kJ/mol and the internal energy E_{int} of $CO(CN)_2$ can be neglected owing to the efficient cooling in the supersonic expansion. The bond dissociation energy D_0(NC–COCN) has been predicted to be 410 kJ/mol based on recent ab initio calculations [8] and experimental findings [6] yielding a value of 209 kJ/mol for E_{avl}. This is partitioned among the photofragment degrees of freedom according to $E_{avl} = E_{int}(\mathrm{CN}) + E_{int}(\mathrm{OCCN}) + E_{trans}(\mathrm{CN}+\mathrm{OCCN})$, where E_{int} consists of the rovobrational excitation. The mean rotational energy of the CN fragment $\langle E_{rot}\rangle = 19.4$ kJ/mol was obtained by summing over the rotational excitation in each populated vibrational state, $\langle E_{rot}\rangle = \sum_v \langle E_{rot}\rangle_v = \sum_{v,J} P_v(J) E_{rot}(J)$, where $P_v(J)$ is the state distribution and $E_{rot}(J)$ is the energy of a given rotational state in the selected vibrational level. The mean vibrational excitation energy, $\langle E_{vib}\rangle = 15.1$ kJ/mol, was calculated in a similar fashion from $\langle E_{vib}\rangle = \sum_v P(v) E_{vib}(v)$. Thus the average rotational and vibrational energy is $\langle E_{int}(\mathrm{CN})\rangle = 34.5$ kJ/mol. Furthermore by PTS, the average translational energy of the fragment pair, $\langle E_{trans}(\mathrm{CO}+\mathrm{OCCN})\rangle$, was measured to be 37 kJ/mol [6]. Table 1 summarizes these findings. Based on these results the internal energy of OCCN, $\langle E_{int}(\mathrm{OCCN})\rangle$, becomes 137.5 kJ/mol and hence 65.8% of the available energy is channeled into internal energy of the OCCN product. In addition, from $E_{trans}(\mathrm{CO}+\mathrm{OCCN})$ one finds $E_{trans}(\mathrm{CN}) = 25$ kJ/mol which corresponds to $T_t \approx 2050$ K in close agreement with the rotational temperature (Fig. 3).

3.3. Rotational alignment and linewidth measurements

Polarization measurement was carried out to determine the rotational alignment (μ, J correlation) [16] of the CN fragment from $CO(CN)_2$ dissociation. For the rotationally cold and hot distributions the rotational alignment $A_0^{(2)}$ was found to be zero to within experimental error. In addition rotational bands with high J from hot CN($v = 0$) fragments were probed to measure their lineshape. Due to the nature of the electronic $^2\Sigma^+ - {}^2\Sigma^+$ transition, these lines are split by the spin-rotation interaction into two components separated by a few tenths of a wavenumber [13]. Each component has a linewidth of ~ 0.13 cm^{-1} corresponding to a translational energy of roughly 30 kJ/mol consistent with the *mean* value of 37 kJ/mol determined by PTS [6].

Table 1
CN product state distributions from 193 nm photodissociation of $CO(CN)_2 \rightarrow \mathrm{CN}(v,J) + \mathrm{OCCN}$

Vibrational level	$P(v)$ experiment	E_{vib} (kJ/mol)	$\langle E_{rot}\rangle$ (kJ/mol)
0	0.58 ± 0.03	0	11.1
1	0.26 ± 0.03	6.4	5.2
2	0.12 ± 0.03	5.8	2.3
3	0.04 ± 0.03	2.9	0.8
Σ	1.00	15.1	19.4

4. Discussion

4.1. Origin of the rotationally hot and cold CN fragments

After excitation at 193 nm, $CO(CN)_2$ has previously been shown to decay with a yield of 94% along a radical channel to CN + OCCN (1a) while the rest of 6% undergoes a molecular decay to $CO + (CN)_2$ [6] as illustrated in Fig. 1. In the present study we investigated exclusively the radical channel by probing the nascent product CN with respect to the rotational and vibrational energy distributions resulting in the energy partitioning presented in Table 2. This is strongly dominated by the internal energy of the CN (34.5 kJ/mol) and OCCN (137.5 kJ/mol) fragment pair which amounts to 82% of E_{avl}. The α-cleavage (1a) generates hot CN fragments with $T_r = 2300$ K and vibrational excitation up to $v = 3$ together with strongly excited OCCN fragments whose average internal energy thus exceeds the dissociation energy for the decay of OCCN to CO + CN which has been calculated by ab initio methods to be 126 kJ/mol [8]. Accordingly, the observed cold CN fragments with $T_r = 410$ K and exclusively in $v = 0$ are attributed to this spontaneous, secondary decay in agreement with the proposal advanced by the PTS results [6]. It is expected that from the 137.5 kJ/mol of E_{int}(OCCN) mainly the vibrational degrees of freedom will contribute to this unimolecular decay. Thus if a statistical energy distribution in OCCN is assumed, we find $E_{vib}(OCCN) = 114$ kJ/mol and $E_{rot}(OCCN) = 28.5$ kJ/mol indicating that only the slow OCCN fragments possess sufficient suitable energy to overcome the barrier consistent with the relatively small amount ($18 \pm 2\%$) of cold CN observed.

The present results of the energy partitioning of E_{avl} among the degrees of freedom of the two fragments given in Table 2 allows us to examine the nature of the decay in terms of the two limiting models, the impulsive and the statistical one. For the former we applied the treatment of Tuck [17] in the soft (OCCN)-stiff (CN) approach; the latter which is based on a randomization of E_{avl} prior to dissociation, has been described extensively in the literature [18]. A comparison with the experimental data clearly favors a statistical fragment state distribution (Table 2). This appears not to be unexpected in view of the fact that the translational fragment energy, usually favored in an impulsive dissociation process, is not dominant, the rotational and vibrational state distributions follow a Boltzmann distribution, and the recoil anisotropy or the rotational alignment is completely lost [19]. However a complete randomization over all the degrees of freedom seems not to be fully achieved since the rotation and translation of the CN probe assume a temperature of 2000–2300 K but that of the vibration is significantly higher with $T_v = 3600$ K.

In this context we mention the photodissociation of acetyl cyanide at 193 nm [20–22]. This decay is dominated by $CH_3COCN \rightarrow CH_3CO + CN$; the yield for breaking of the weaker $C–CH_3$ bond is only about 15%. The LIF analysis of the CN fragment by Horwitz et al. [20] has shown the rotational and vibrational state distribution to be described by $T_r \sim T_v \sim 1800$ K. Similar to $CO(CN)_2$ the internal energy partitioning of CH_3COCN follows approximately a statistical distribution as would be expected from similar mechanistic decay feature of the two molecules.

Table 2
Product energy partitioning (kJ/mol) from 193 nm photodissociation of $CO(CN)_2$ applying different models[a]

	E_{rot} (CN)	E_{vib} (CN)	E_{trans} (CN)	E_{int} (OCCN)	E_{trans} (OCCN)
Impulsive[bc]	3.6	0	74.6	81.8	49.6
Statistical	19.1	19.1	19.2	142.5	9.3
Experiment	19.4	15.1	25[d]	137.5[e]	12[d]

[a] $E_{avl} = h\nu - D_0(NC–COCN) = 209$ kJ/mol. [b] 'Soft OCCN'–'rigid CN' impulsive model was used. [c] Geometry taken from the ground state of the parent molecule in Ref. [8]. [d] The values of E_{trans}(CN) and E_{trans}(OCCN) from Ref. [6]. [e] From $E_{avl} - E_{int}(CN) - E_{trans}$(total).

4.2. Mechanistic aspect

Following excitation the α-cleavage of $CO(CN)_2$ is indicated to be indirect and slow compared to the parent rotation. The absence of a direct impulsive bond scission at an excitation energy of 619 kJ/mol is unexpected and suggests a very efficient internal conversion from the initially prepared state which is either a $^1(n, 3s)$ Rydberg [23] or as recently suggested a $\pi_{CN}\pi^*_{CO}$ state [24], to lower excited states or the ground state S_0. It is conceivable that a sequence of conical intersections [25,26] is involved so that the dissociation takes place from the S_0 surface as has been assumed in the ab initio study [8]. The calculation predicts $D_0(NC–COCN) = 410$ kJ/mol and no energy barrier in the exit channel. The primary OCCN fragments possess sufficient internal energy so that a part, accounting for 18% of all the CN fragments, decays spontaneously to essentially cold CO + CN fragments. Parallel to the PTS results no evidence for a concerted three body process has been found.

Acknowledgements

This work was supported by the Swiss National Science Foundation. The authors thank Rolf Pfister for the synthesis of carbonyl cyanide and Dr. Alan Furlan for helpful discussions.

References

[1] S.W. North, D.A. Blank, J.D. Gezelter, C.A. Longfellow, Y.T. Lee, J. Chem. Phys. 102 (1995) 4447.
[2] K.A. Trentelman, S.H. Kable, D.B. Moss, P.L. Houston, J. Chem. Phys. 91 (1989) 7498.
[3] S.K. Kim, S. Pedersen, A.H. Zewail, J. Chem. Phys. 103 (1995) 477.
[4] J.C. Owrustsky, A.P. Baronavski, J. Chem. Phys. 110 (1999) 11206.
[5] C. Maul, K.-H. Gericke, Int. Rev. Phys. Chem. 16 (1997) 1.
[6] H.A. Scheld, A. Furlan, J.R. Huber, J. Chem. Phys. 111 (1999) 923.
[7] W.H. Green, C.B. Moore, W.F. Polik, Ann. Rev. Phys. Chem. 43 (1992) 591.
[8] H.U. Suter, J.R. Huber, T.-K. Ha, Chem. Phys. Lett. 311 (1999) 474.
[9] R. Pfister, J.R. Huber, unpublished results.
[10] M. Dubs, U. Brühlmann, J.R. Huber, J. Chem. Phys. 84 (1986) 3106.
[11] M.P. Docker, A. Ticktin, A. Brühlmann, J.R. Huber, J. Chem. Soc. Faraday Trans. 2 85 (1989) 1169.
[12] W.J. Linn, O.W. Webster, R.E. Benson, J. Am. Chem. Soc. 87 (1965) 3651.
[13] C.V.V. Prasad, P.F. Bernath, J. Mol. Spectrosc. 151 (1992) 459.
[14] B. Brocklehurst, G.R. Hebert, S.H. Innanen, R.M. Sell, R.W. Nicholls, Identification Atlas of Molecular Spectra, vol. 9, York University, Centre for Research in Experimental Space Science, Toronto, 1972.
[15] J. Luque, D.R. Crosley, LIFBASE: Database and Spectral Simulation Program (Version 1.5), SRI International Report MP 99-009, 1999.
[16] R.N. Dixon, J. Chem. Phys. 85 (1986) 1866.
[17] A.F. Tuck, J. Chem. Soc. Faraday Trans. 2 73 (1977) 689.
[18] J.T. Muckerman, J. Phys. Chem. 93 (1989) 179, and references therein.
[19] S. Yang, R. Bersohn, J. Chem. Phys. 61 (1974) 4400.
[20] R.J. Horwitz, J.S. Francisco, J.A. Guest, J. Phys. Chem. A 101 (1997) 1231.
[21] S.W. North, A.J. Marr, A. Furlan, G.E. Hall, J. Phys. Chem. A 101 (1997) 9224.
[22] A. Furlan, H.A. Scheld, J.R. Huber, J. Phys. Chem. A 104 (2000) 1920.
[23] M.B. Robin, Higher Excited States of Polyatomic Molecules, Academic, New York, 1975, for carbonyl cyanide in analogy to other carbonyl compounds.
[24] J.C. Owrutsky, A.P. Baronavski, J. Chem. Phys. 111 (1999) 7329.
[25] M. Klessinger, Angew. Chem. Int. Ed. Engl. 43 (1995) 549.
[26] W. Domcke, G. Stock, Adv. Chem. Phys. 100 (1997) 1.